AMERICAN UNIVERSITY OF BEIRUT

LIQUID PHASE SULFUR PASSIVATED NICKEL CATALYST FOR DRY REFORMING OF METHANE

by

GHADEER ALKHANSA

A thesis
submitted in partial fulfillment of the requirements
for the degree of Master of Engineering
to the Department of Chemical and Petroleum Engineering
of the Maroun Semaan Faculty of Engineering and Architecture
at the American University of Beirut

Beirut, Lebanon
September 2018

AMERICAN UNIVERSITY OF BEIRUT

LIQUID PHASE SULFUR PASSIVATED NICKEL CATALYST FOR DRY REFORMING OF METHANE

by

GHADEER ALKHANSA

Approved by:

Dr. Mohammad N. Ahmad, Professor, Chairman — Advisor
Department of Chemical and Petroleum Engineering

Dr. Joseph Zeaiter, Professor — Co-Advisor
Department of Chemical and Petroleum Engineering

Dr. Mu'Tasem Shehadeh, Professor — Member of Committee
Department of Mechanical Engineering

On his behalf
Dr. Belal Abu Tarboush, Professor — Member of Committee
Department of Chemical and Petroleum Engineering

Date of thesis defense: September 11, 2018

AMERICAN UNIVERSITY OF BEIRUT

THESIS, DISSERTATION, PROJECT RELEASE FORM

Student Name: Alkhansa Ghadeer Mohsen
Last First Middle

(✓) Master's Thesis ( ) Master's Project ( ) Doctoral Dissertation

[ ] I authorize the American University of Beirut to: (a) reproduce hard or electronic copies of my thesis, dissertation, or project; (b) include such copies in the archives and digital repositories of the University; and (c) make freely available such copies to third parties for research or educational purposes.

[✓] I authorize the American University of Beirut, to: (a) reproduce hard or electronic copies of it; (b) include such copies in the archives and digital repositories of the University; and (c) make freely available such copies to third parties for research or educational purposes
after:

One ---- year from the date of submission of my thesis.
Two ---- years from the date of submission of my thesis.
Three ---- years from the date of submission of my thesis. ✓

Ghadeer 13/9/2018

Signature Date

ACKNOWLEDGEMENTS

I would like to thank my family and friends for supporting me and being there for me throughout my thesis journey. And special thanks for Nicolas Aramouni for his collaboration on the project. Finally, I would like to thank my advisors Dr. Mohammad Ahmad and Dr. Joseph Zeaiter for guidance, and the Lebanese Council for Scientific Research (LCNRS) for funding the project.

AN ABSTRACT OF THE THESIS OF

Ghadeer Alkhansa for Master of Engineering

Major: Chemical Engineering

Title: Liquid Phase Sulfur Passivation of Nickel Catalyst for Dry Reforming of Methane

Dry reforming of methane (DRM) utilizes the two most abundant greenhouse gases: carbon dioxide (CO_2) and methane (CH_4) to produce a useful syngas mixture of carbon monoxide (CO) and hydrogen (H_2). DRM operates at high temperatures (>700℃). Thus, the traditional Ni-based catalyst used for the reforming reaction is subjected to deactivation due to coke formation and especially due to the formation of carbon whiskers. These whiskers will grow in the pores of the catalyst pellets leading to their destruction. It was shown that sulfur passivation of the catalyst during the reaction, by introducing small amounts of hydrogen sulfide gas (H_2S), blocks carbon formation while allowing the reforming reaction to take place. In an attempt to improve the currently proposed gas phase sulfur passivation process, sulfur was introduced as liquid phase during the synthesis of the catalyst to eliminate the use of gaseous H_2S in coating the catalyst. Partially covered nickel catalysts with different sulfur concentrations were tested in the reformer. Characterization of fresh and spent catalysts were done by XRD, TGA, BET and SEM analysis. A compromise on CH_4 and CO_2 conversions of 21% and 27% respectively with 80% loss in carbon formed on the catalyst surface resulted from a sulfur concentration of 80 ppm (12% coverage). The carbon deposited was in the form of undeveloped whiskers called “octopus carbon”.

Keywords: Dry reforming, Nickel catalyst, coke formation, sulfur passivation, liquid/solid adsorption.

CONTENTS

ACKNOWLEDGEMENTS v

ABSTRACT vi

LIST OF ILLUSTRATIONS ix

LIST OF TABLES x

Chapter

I. INTRODUCTION 1

II. LITERATURE REVIEW 3

A. Nickel Based Catalyst 3
B. Catalyst Deactivation 4
1. Coke Formation 4
2. Metal Sintering 5
3. Sulfur Poisoning 5
C. Sulfur passivation 6
1. The Concept 6
2. SPARG Process 7

III. EXPERIMANTAL PROCEDURE 8

A. Materials 8
B. Catalyst Preparation 8
C. Catalyst Characterization 9
1. X-ray diffraction (XRD) analysis 9
2. Nitrogen Adsorption Analysis 9
3. Thermogravimetric analysis (TGA) 9
4. SEM Analysis 10
D. Liquid Phase Sulfur Passivation 10
E. DRM Reaction 11

IV. RESULTS AND DISCUSION 12

A. Adsorption Isotherm 12
B. Characterization of Fresh Catalysts 14
1. X-ray Diffraction (XRD) Analysis 14
2. N_2 Adsorption Results 15
C. Catalyst Activity 16
D. Characterization of Spent Catalysts 20
1. TGA Analysis 20
2. SEM results 22
E. Choosing the Best Catalyst 23
V. CONCLUSION 25
REFERENCES 27

ILLUSTRATIONS

Figure Page

1. Adsorption Isotherm at 50 °C showing the sulfur coverage on nickel surface as a function of sulfide concentration added 13
2. XRD patterns for 8 wt% Ni-10 wt%MgO-Al_2O_3 fresh catalyst 14
3. Methane and CO_2 conversion for catalysts with different sulfur concentration after 3h reaction and GHSV=48,000 ml/g_{cat}/h. 17
4. H_2/CO ratio for catalysts with different sulfur concentrations after 3h reaction and GHSV=48,000 ml/g_{cat}/h. 18
5. (a) CH_4 conversion, (b) CO_2 conversion, (c) H_2 yield, and (d) CO yield of catalysts with different sulfur concentrations as a function of time. 19
6. TGA results of spent catalyst with different sulfur concentrations (a) weight loss as function of temperature (b) coke formed as function of sulfur concentration.....20
7. SEM Images of Spent Catalyst (a) S_0, (b) S_{80}, (c) S_{160}, and (d) S_{1500} 22
8. Methane conversion and coke formed as a function of sulfur concentration 23

TABLES

Table Page

1. BET surface areas, pore volumes, and pore sizes of fresh catalysts with different sulfur concentrations 15

CHAPTER 1

INTRODUCTION

With the rise of the economic and technological development in societies, energy demand has been increasing significantly to provide basic living conditions. Fossil fuel, which is the most abundant energy source, has a considerable influence on the environment since burning it leads to the emission of carbon dioxide (CO_2) and other greenhouse gases (GHG) [1, 2]. Hydrogen, on the other hand, appears to be a viable, eco-friendly alternative energy source [3, 4]. It is produced from synthesis gas (syngas) that is manufactured through processes called "Reforming".

Dry reforming of methane (DRM), represented by reaction (1), is one of the routes considering the production of syngas by utilizing the most two abundant greenhouse gases CO_2 and methane (CH_4) [2, 4, 5]. The syngas produced, a mixture of carbon monoxide (CO) and hydrogen, has a H_2/CO ratio of unity which makes it a key intermediate in the chemical industry. The syngas can be used in synthesis of oxygenated chemicals, specially ammonia and methanol, synthetic fuels, and in Fischer–Tropsch process [6, 7].

$$CH_4 + CO_2 \rightarrow 2CO + 2H_2 \qquad (\Delta H = +\frac{247kJ}{mol}) \qquad \text{(rxn-1)}$$

Transition Metal based catalyst (i.e. nickel (Ni)) is used in the reforming reaction. Being a highly endothermic reaction, high temperature is required for the DRM reaction to take place (>700°C)[2] , which puts the catalyst in risk of being destroyed due to the formation of whisker carbon [8].

SPARG (Sulfur PAssivated ReforminG) process is currently used as a commercial process that utilizes DRM preventing coke formation [9]. It is based on the findings of Rostrup-Nielsen [10] who described that coke formation needs an ensemble of nickel atoms larger than that required for the reforming reaction to take place. Hydrogen sulfide gas (H_2S) is introduced in the reformer and sulfur chemisorbs on the surface Ni and blocks some active sites [10]. Sulfur coverage of 70% of the Ni surface area is proven to inhibit carbon formation allowing on the other hand the reforming reaction to take place [10, 11].

However, the presence of H_2S in the gas feed creates a substantial risk of corrosion and requires more expensive materials of construction. H_2S adsorbs strongly on metallic tubes [12]. Moreover, H_2S should be introduced throughout the reaction so that any slight change in its partial pressure will affect the coverage significantly. This will reflect negatively on the conversion and yield and requires precise process control.

In an attempt to improve the currently proposed process, it is desirable to eliminate the use of gaseous H_2S to coat the catalyst. Therefore, sulfur was introduced in the liquid phase during the synthesis of the catalyst and tested directly in the reformer in a sulfur-free feed gas. The catalyst was synthesized using a sol-gel method since the xerogel catalyst displayed high surface area, high porosity and small distribution of particle size leading to a very high activity [13]. They also showed high coke resistance compared to those prepared by other methods [14]. Since the liquid phase adsorption of sulfur on nickel and alumina is poorly studied, an adsorption isotherm for the system was developed, from which relevant data about sulfur coverage was obtained. Then the catalysts with different sulfur coverages were tested in a reformer and characterized before and after reaction.

CHAPTER II

LITERATURE REVIEW

A. Nickel Based Catalyst

For the past decades, chemical engineers have been trying to develop a highly stable and active catalyst for DRM by using different types of active materials and supports, and by trying different synthesis methods [2].

Transition metals of groups 8,9, and 10 of the periodic table are the best candidates for DRM catalyst. Although noble metals, such as Pt, Ru, and Rh, create a highly active and stable catalyst material, they are economically infeasible. On the other hand, Ni-based catalyst, which is also highly reactive, is much cheaper and more available which makes it the most frequently reported material for DRM catalyst [2, 4, 15, 16].

Metal oxides are used as supports for the Ni catalyst. Aluminum oxide (Al_2O_3) is one of the commonly used supports since it provides a highly active surface area, high thermal stability, and is relatively cheap [15]. Magnesium oxide (MgO) is often added to the support to enhance the resistance to coke formation in DRM, owing to its basic property [17, 18]. Studies showed that a proper mixing of MgO and Al_2O_3 matrices for Ni- catalyst gives a more active and highly stable catalyst than using each support alone. A typical loading of 8-10% Ni and 10-15%MgO gave optimal results [14, 18, 19].

B. Catalyst Deactivation

Unlike noble metals, Ni-based catalyst deactivate easily at high temperatures and in the presence of hydrocarbons due to coke formation, metal sintering, and sulfur poisoning [20].

1. Coke Formation

Two main side reactions are known to be responsible for carbon formation in DRM: decomposition of CH_4 (reaction 2) and disproportionation of CO, known as Boudouard reaction, (reaction 3) [5, 9, 21-24].

$$CH_4 \rightarrow C + 2H_2 \qquad (\Delta H = +75\frac{kJ}{mol}) \qquad \text{(rxn-2)}$$

$$2CO \rightarrow C + CO_2 \qquad (\Delta H = -172\frac{kJ}{mol}) \qquad \text{(rxn-3)}$$

The coke may grow on the nickel catalyst in various forms depending on the specific conditions of the reaction taking place. Each form has a unique characteristic and effect on the catalyst [9]. At elevated temperatures, the carbon deposits formed during these reactions dissolve in the metal particle and nucleate at the rear metal-support interface to form whiskers or fibers under the small Ni particles .Having a high mechanical strength, those carbon whiskers lead to the breakdown of the catalyst particles/pellets and the blockage of the reformer tube [8, 10]. Catalyst regeneration is not an option in this case [25].

Particle size plays a crucial role in carbon nucleation. A minimal size of Ni-crystallites of 7 nm is needed for the formation of whisker carbon. So small Ni particles are less prone to carbon formation [26]. Hence it is essential when manufacturing a catalyst to achieve high dispersion of the active phase.

2. *Metal Sintering*

Sintering is the coalescence of small particles into larger particles leading to the loss of catalytic surface area and support area. During sintering the crystallites grow in size which reduces the available metal atoms for reaction and the pores of the support collapse, trapping crystallites of the active phase in the pores [25, 27]. Thus, sintering affects both activity and stability of the catalyst.

Many parameters affect the rate of sintering such as: reaction temperatures, the atmosphere over the catalyst, and the metal support type. Sintering takes place at high temperatures and its rate accelerates exponentially with increasing temperature [28]. The rate of sintering is also enhanced with presence of water vapor [29]. In DRM, it is essential to work at high temperatures. Although the atmosphere is dryer than in steam reforming, the production of steam (H_2O) by the reverse water-gas shift side reaction (RWGS) (reaction 4) cannot be avoided, and therefore the risk of sintering is significant [30].

$$CO_2 + H_2 \rightarrow CO + H_2O \qquad \left(\Delta H = +\frac{70kJ}{mol}\right) \qquad \text{(rxn-4)}$$

the only way to minimize sintering is therefore by ensuring a strong metal-support interaction. The addition of MgO to the support during the Ni catalyst preparation leads to the formation of spinel NiO-MgO. This mixed oxide phase results in increasing metal-support interaction, thus reduces catalyst deactivation via sintering [2, 31].

3. *Sulfur Poisoning*

Sulfur is a common poison for nickel in reforming processes. It adsorbs strongly on nickel leading to its deactivation [20]. Therefore, desulfurization of the feed gas should always take place before the gas is introduced to the reformer.

Desulfurization is a two-step process where the sulfur-containing compounds are hydrogenated to form hydrogen sulfide, which is then adsorbed on zinc oxide (ZnO) [32].

C. Sulfur passivation

Developing a coke resistant nickel catalyst has been a challenge. Different approaches have been considered. An interesting approach, proposed by Rostrup-Nielsen, is the sulfur passivation of surface Ni to inhibit coke deposition [23].

1. The Concept

Sulfur, a known catalyst poison, chemisorbs on nickel to form well-defined two dimensional surface sulfides that forms very strong bonds with surface nickel compared to the bond between surface and bulk nickel [33]. One sulfur atom can quench around two neighboring nickel atoms [10].

Rostrup-Nielsen [10] studied the effect of partial sulfur passivation of surface nickel on DRM by introducing a small amount of H_2S gas in the reformer feed. He showed that there exists threshold sulfur coverage of 70 % at which carbon formation is minimized and the catalyst activity is acceptable. Below this coverage, carbon formation is not inhibited, and the catalyst activity slightly reduces. In contrast, above the threshold, the catalyst activity drops significantly [10]. This is because sulfur inhibits the dissociation of carbon monoxide (the Boudouard reaction) [23, 34] that requires an ensemble of four simultaneous Ni atoms to take place [35-38]. This ensemble is larger than that required for the reforming reaction (3 atoms) [10, 39]. However, amorphous carbon structures are still formed and a new form of whisker

carbon, called octopus carbon, could also be produced [10]. These forms of carbon are less destructive, although they cause a loss of activity. However, the catalyst can be regenerated. The basis of the ensemble size control was first found in the work of Alstrup et al. on sulfur adsorption on nickel. They developed an expression for sulfur coverage, represented by equation (1)

$$\theta = 1.45 - 9.53 * 10^{-5}.T + 4.17 * 10^{-5}.T.\ln\left(\frac{P_{H_2S}}{P_{H_2}}\right) \quad (1)$$

where θ is the sulfur fractional coverage, T is the temperature in degree K, and P_{H_2S} and P_{H_2} are the partial pressures of H_2S and H_2 respectively [39].

2. SPARG Process

On the basis of the promising results of sulfur passivation, the scale-up from fundamental studies to pilot testing led to the introduction of the SPARG process to industry [40]. The sulfur passivated reforming process(SPARG) , developed by Haldor Topsoe [41] , was first commercialized at Sterling's Texas City plant in 1987 [42] for steam reforming of methane (SRM). In SPARG, The amount of H_2S in the feed stream is controlled to block the carbon nucleation sites of the catalyst by chemisorbing on the step sites of the Ni particles [7, 41].

Building on the success of the first industrial plant, SPARG was used for DRM. Starting with desulfurization of the natural gas (NG), followed by a pre-reformer for the removal of high hydrocarbons to avoid cracking on sulfur passivated catalyst, a CO_2/NG feed ratio of 2.5 enters the reformer with a H_2S/H_2 ratio <0.9 (to avoid the formation of bulk nickel sulfide) [43]. Carbon free-operation was established during 4 years of continuous operation on one batch of catalyst [42] to produce a CO-rich syngas that could be used in the synthesis of the acetic acid, dimethyl ether, and for the direct reduction of iron [41].

CHAPTER III

EXPERIMANTAL PROCEDURE

A. Materials

Nickel (II) nitrate hexahydrate (≥ 97%), Magnesium ethoxide (98%), and Aluminum-tri-sec-butoxide (ATB) (97%), provided by Sigma-Aldrich, were used as catalyst precursors. Sec- butanol (≥ 99%), provided by Sigma-Aldrich, was used as solvent so that gelation occurred in the absence of added water [44]. Acetic Acid (AA) (100%) and nitric acid (65%), provided by VWR, were used as chelating and hydrolyzing agents respectively. Lithium sulfide (99.98%), provided by Sigma-Aldrich, was used as a sulfur source since it is highly soluble in water.

B. Catalyst Preparation

Preparation of 8 wt.% Ni/10 wt%MgO-Al_2O_3 catalyst was prepared using sol-gel method to ensure a high surface area, a high porosity, a small distribution of particle size, and a high catalytic activity [13, 14, 45]. ATB was dissolved in sec-butanol, so that the concentration is 1M, for 30 min. at 70°C. Magnesium ethoxide was then added and mixed for 30 min. at the same temperature. Acetic acid was added so that the molar ratio of AA to ATB was 1:1 to get a transparent sol [44]. After 30 min., nitric acid (65%) was added dropwise at 60°C until pH=3 and mixed for two hours. Finally, the nickel precursor was added and left to mix for another 30 min.; a green gel was formed. The gel was aged in a Teflon-lined autoclave at 110°C for 43 hours. The sample was

then filtered, washed with deionized water, and dried at 80°C for 30 hours before being calcined in air at 650°C for 5 hours.

C. Catalyst Characterization

1. X-ray diffraction (XRD) analysis

A Bruker D8 Advance diffractometer, equipped with a Cu-Kα irradiation source, was used for XRD measurements. Phase identifications were carried out by comparing the collected spectra with spectra in the database. The particle size diameter was estimated using the classical Scherrer equation (equation 2).

$$d = \frac{K*\lambda}{\beta*\cos(\sigma)} \tag{2}$$

where d is the crystallite diameter (nm), λ is the wavelength of the x-ray ($\lambda = 0.15406$ nm), σ is the Bragg angle, K is Scherrer constant and its related to the crystallite shape (K is between 0.8 and 1.39), and β is the full width at half maximum (FWHM) in radiance [46].

2. Nitrogen Adsorption Analysis

A micromeritics Gemini VII instrument was used to measure the BET surface area, BJH pore volume, and BJH pore size of the fresh catalyst by nitrogen adsorption-desorption at 77K. Prior to analysis, the sample was degassed at 120°C for 5 hours then immersed in liquid N_2 to cool to 77K.

3. Thermogravimetric analysis (TGA)

TGA analysis of the spent and fresh catalysts were performed on a TA Q500 instrument. Samples were heated at 15 °C/min until 900°C in N_2.

4. SEM Analysis

Scanning Electron Microscope (SEM MIRA 3 LMU Tescan, Czech Republic) was used to visualize the whiskers formed. Samples of spent catalysts were coated with gold using Q150 T Turbo - Pumped Sputter Coater (Quorum Technologies). The samples were then placed into the SEM sample holder. The working distance between the lenses and the sample is 10 mm to 16 mm, with an acceleration voltage of 20 kV and using an in-beam detector at a magnification range from 20K to 50K.

D. Liquid Phase Sulfur Passivation

Different concentrations of sulfide solutions were prepared by dissolving lithium sulfide in sodium hydroxide solution with a pH>13 to avoid formation of H_2S fumes [47]. For each concentration, 3 ml of solution was in contact with 30-40 mg catalyst at 50◦C for 45min [48]. Then, solid-liquid separation was done by centrifugation. To calculate the amount of sulfur adsorbed, the concentration of sulfur in the solution before and after contact with the catalyst was determined based on Spectrophotometric Methylene Blue Method (USEPA Method 8131) where sulfide reacts with two reagents containing ferric chloride, and N, N-dimethyl-*p*-phenylenediamine to form methylene blue. A measurement wavelength of 665 nm for spectrophotometers measures the intensity of the blue color which is proportional to the sulfide concentration [49]. A HACH DR6000 spectrophotometer, with the installed software Sulfide 690, was used for this purpose. The sulfur uptake on the nickel catalyst was then calculated using equation 3.

$$q = \frac{[S]_i - [S\}_f}{m_{cat}} \tag{3}$$

where q is the sulfur uptake on nickel surface (ppm S/ mg catalyst), $[S]_i$ and $[S]_f$ are the concentrations of sulfur in Li_2S solution before and after adsorption respectively (ppm) (their difference is concentration of S adsorbed) and m_{cat} is the mass of catalyst (mg).

E. DRM Reaction

Activity test was carried out in a 4 mm ID quartz tube inside a horizontal tubular furnace, under atmospheric pressure, in which 10-15mg catalyst is packed supported by inert quartz wool plugs. Prior to the reaction, the catalysts were reduced in situ at 700°C for 30 min in flowing mixture of 20%H_2/N_2 with a flow rate of 10ml/min. Methane and CO_2 were then fed in equimolar amounts to the tube using Brooks 4800 Series flow controllers. The reaction took place at 800°C with a total flow rate of 8ml/min. Product gases were analyzed using an Agilent 7820 gas chromatograph (GC) installed in-line with a 6-port gas sampling valve using a thermal conductivity detector and a Porapak Q porous polymer column. Argon was used as carrier gas at a flow rate of 20 ml/min. Elution was performed at a constant temperature of 50 °C. A new measurement was taken every 5 min. for short run experiments, and every 15 min. for long run experiments. The methane conversion (X_{CH_4}), CO_2 conversion(X_{CO_2}), H_2 yield (Y_{H_2}), and CO yield (Y_{CO}) where determined by the following formulas:

$$X_{CH_4} = \frac{CH_{4in} - CH_{4out}}{CH_{4in}} * 100 \quad (4)$$

$$X_{CO_2} = \frac{CO_{2in} - CO_{2out}}{CO_{2in}} * 100 \quad (5)$$

$$Y_{H_2} = \frac{H_{2in} - H_{2out}}{H_{2in}} * 100 \quad (6)$$

$$Y_{CO} = \frac{CO_{in} - CO_{out}}{CO_{in}} * 100 \quad (7)$$

CHAPTER IV

RESULTS AND DISCUSION

A. Adsorption Isotherm

The study of chemisorption of sulfur on Ni catalyst has been of interest since sulfur is a main poison during reforming[34, 50-52]. Adsorption is described through isotherms that reflects amount of adsorbate taken up by the adsorbent at a constant temperature [53]. There are different equations proposed to describe quantitatively the isotherms e.g. Langmuir model. The main assumptions in this model are a constant adsorption energy over all sites, a localized adsorption on the surface, and a monolayer adsorption [54].

Researchers have been studying the gas-solid adsorption of H_2S (g) on nickel since the 1960's [10, 39, 42, 52, 55, 56]; however, no records of liquid-solid adsorption isotherm of sulfide on nickel have been found.

To do an adsorption isotherm, the sulfur uptake at different sulfur concentrations was calculated by dividing the amount of sulfur adsorbed on the catalyst by the mass of the catalyst. Since the type of adsorption between sulfur and Ni is chemisorption[33], a monolayer of sulfur atoms adsorb on Ni surface [57]; accordingly, the data of the uptake versus sulfur concentration was fitted to Langmuir's model, represented by equation 8, using the curve fitting toolbox on Matlab.

$$q = \frac{q_{max} * K * [S]}{1 + K * [S]} \tag{8}$$

where q and q_{max} are the uptake and maximum uptake respectively (ppm S/mg cat.), [S] is the concentration of sulfur in lithium sulfide added (ppm), and K is the Langmuir

constant (ppm^{-1}). A maximum uptake of 6 ppm/mg catalyst and a Langmuir constant of 0.002 ppm^{-1} were obtained with a 0.947 coefficient of determination (R^2).

The surface coverage θ was calculated using equation 9 and plotted versus sulfur concentration to obtain an adsorption isotherm of sulfur on the Ni based catalyst at 50°C represented by figure 1.

$$\theta = \frac{q}{q_{max}} * 100 \quad (9)$$

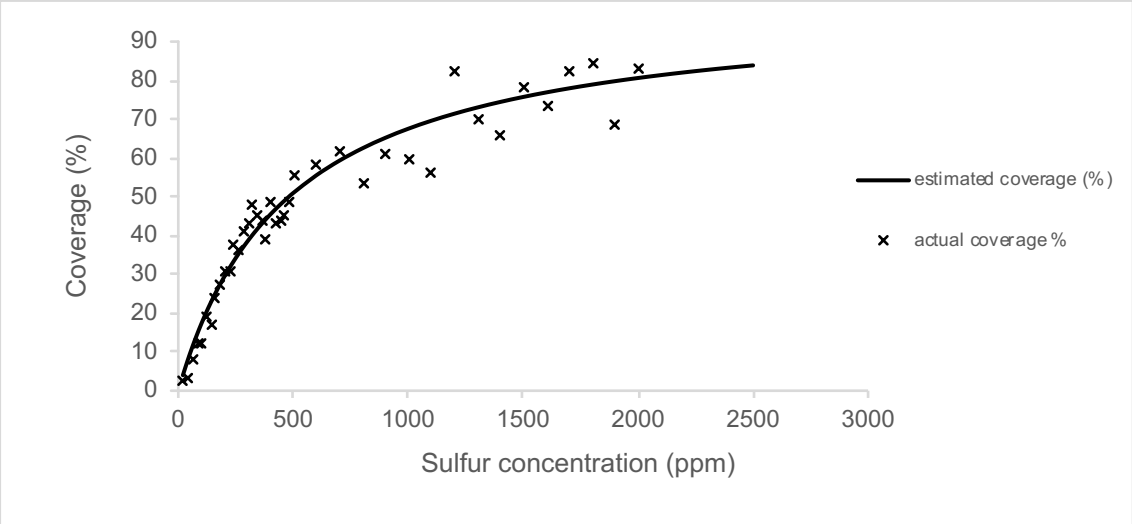

Figure 1- Adsorption Isotherm at 50 °C showing the sulfur coverage on nickel surface as a function of sulfide concentration added

A goodness of fit of 0.947 indicates that Langmuir model is a suitable fit. As for the inaccuracy, it might be due to the experimental errors that arose from using a high dilution factor (above 500 times) specially at high sulfur concentrations as the spectrophotometer reads a maximum of 800 μg/L. A few μL of the sulfide solution must be diluted in 10 ml water, which makes this operation very sensitive to human error.

Besides, Rostrup-Nielsen showed that on average, 0.54 sulfur atoms adsorb per nickel atom which corresponds to a maximum sulfur uptake of 440 ppm S per m^2/g of nickel [52]. From table (BET), the surface area of the prepared catalyst with no sulfur (S_0) is 200 m^2/g, and since the catalyst contain 8% Ni, the Ni surface area can be assumed to be 16 m^2/g. According to the adsorption isotherm derived in equations 8 and 9, 440 ppm S per m^2/g corresponds to approximately 94% coverage, which shows a relatively small deviation from the results of Rostrup-Nielsen.

B. Characterization of Fresh Catalysts

1. X-ray Diffraction (XRD) Analysis

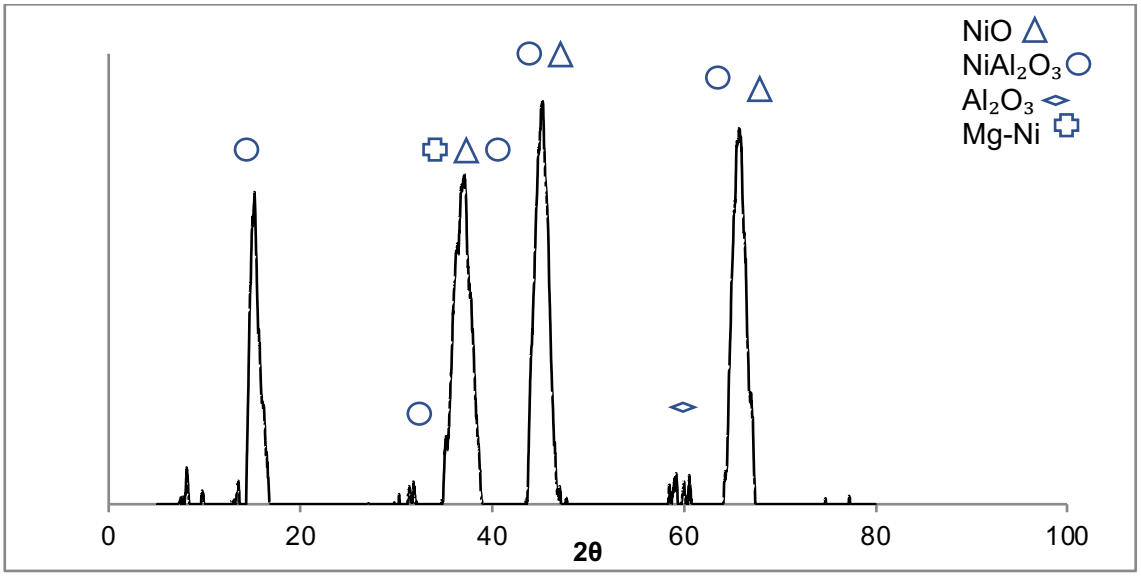

Figure 2- XRD patterns for 8 wt% Ni-10 wt%MgO-Al_2O_3 fresh catalyst

XRD patterns for the fresh catalyst Ni-MgO-Al_2O_3 before reduction are shown in figure 2. Peaks can be observed at 2θ values of 45.28° and 65.84° which correspond to the (1 1 1) and (2 2 0) planes of NiO [58]. $NiAl_2O_3$ peaks overlap with NiO peaks and

can be shown at 2θ value of 15.22°. The formation of this spinel indicates high interaction of nickel and alumina lattice which can suppress carbon deposition and metal sintering during the reforming reaction [59].

Particle size also plays a crucial role in carbon nucleation. A minimal size of Ni- crystallites of 5 nm is needed for the formation of whisker carbon [26]. Using Scherrer equation, and assuming the crystalline is spherical, by taking K to be 0.96 [60], the Ni- crystallites average size is around 5.5 nm. This shows the crystalline has potential for carbon inhibition.

2. *N_2 Adsorption Results*

The nitrogen adsorption results, of five fresh catalyst samples with different sulfur concentrations, are shown in table1. The samples name S_i corresponds to the amount of sulfur added, i.e. "i" is the concentration of sulfur in ppm.

Table 1- BET surface areas, pore volumes, and pore sizes of fresh catalysts with different sulfur concentrations

Sample name	BET surface area (m^2/g)	Pore volume (cm^3/g)	Pore size (nm)
S_0	200	0.463	6.743
S_{500}	212	0.463	6.255
S_{900}	232	0.482	6.453
S_{1400}	262	0.529	5.573
S_{2000}	283	0.574	5.575

The BET surface area, BJH pore volume, and BJH pore size of S_0 200.013 m^2/g, 0.463 cm^3/g, 6.743 nm respectively. As the sulfur content increased, the surface area and pore volume increased, and the pore size decreased to reach 282.745 m^2/g, 0.574 cm^3/g and 5.575 nm respectively for sulfur content of 2000 ppm. The increase in surface area with increase is sulfur concentration is somehow linear. An average of 20 m^2/g increase in area is associated with around 500 ppm increase in sulfur content. This shows that the BET surface area corresponds to the whole catalyst area and not just to the active site. As for the change in pore size and pore volume, can be explained by modifications in the support structure, which might be due the formation of surface sulfate and sulfite compounds that block the pores [61], or due to the formation of bulk sulfide (Ni_3S_2).

C. Catalyst Activity

The effect of sulfur content on the feed conversion after 3-hour reaction is illustrated in figure 3. The CH_4 and CO_2 conversions of the catalyst without sulfur were 56 % and 63% respectively. As sulfur concentration increased, both conversions dropped due to the coverage of the active sites with sulfur. CO_2 conversion was slightly higher until 300 ppm (corresponding to 42% coverage), at which the CH_4 conversion became higher. Conversion continued to decrease until 1100 ppm (corresponding to 70% coverage) where beyond that, conversion remained constant as the sulfur content increased to 2000 ppm, with CH_4 and CO_2 conversions around 2.5 % and 0.0 % respectively.

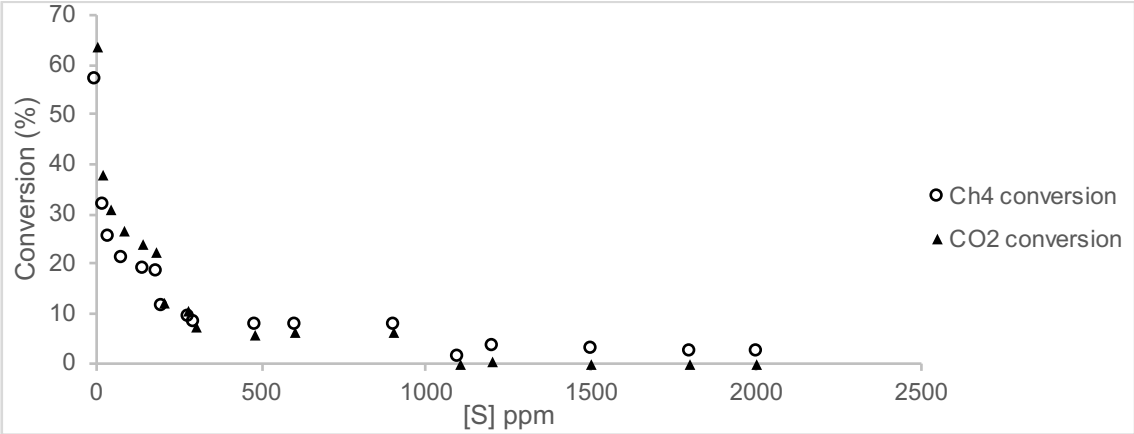

Figure 3- Methane and CO_2 conversion for catalysts with different sulfur concentration after 3h reaction and GHSV=48,000 ml/g_{cat}/h.

The conversion of CO_2 was slightly higher than that of CH_4, at low sulfur concentrations, which is attributed to the simultaneous occurrence of the RWGS reaction (reaction 4) [62, 63]. On the other hand, the high conversion of methane relative to CO_2, at high sulfur coverages, can be explained by two theories.

The first theory is the occurrence of the Boudouard reaction (reaction 3) that lead to the production of CO_2 [57], thus explaining the lower conversion of CO_2 [64]. Studies have shown that there is a competition for sites between the Boudouard reaction and the RWGS reaction, and that the RWGS reaction proceeds much faster [65]. This is why it is dominating at low sulfur coverages. However, at high coverages where the surface area decreased, the Boudouard reaction became more dominant. A possible explanation to this might be that the Boudouard reaction needs less area than RWGS to take place. Further studies are required to fully elaborate this observation.

The second theory is the modification in the structure of the support, especially at high concentrations. Results obtained from XRD and Transmission electron microscopy (TEM) characterization by Silvaiah et al. [66] confirmed that CO_2 conversion depends on the support, whereas CH_4 conversion is sensitive to nickel

particles size. The N_2 adsorption results in table 1 clearly shows that there is a significant change in pore volume and pore size at high sulfur concentrations, thus affecting the CO_2 conversion. XRD analysis should be performed on fresh sulfur passivated catalysts to study the effect of sulfur on Ni particle size.

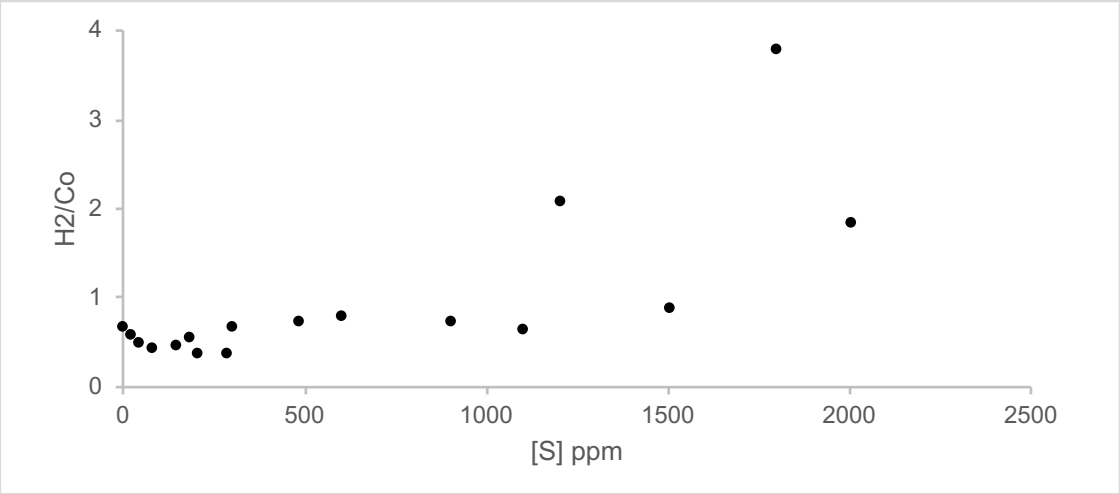

Figure 4- H_2/CO ratio for catalysts with different sulfur concentrations after 3h reaction and GHSV=48,000 ml/g_{cat}/h.

The effect of these two theories, at high sulfur concentrations, can also be seen in figure 4 that illustrates the H_2/CO ratio after 3 hours reaction of catalysts with different sulfur concentrations. Below 1100 ppm, the H_2/CO ratio was less than unity proving the occurrence of the RWGS [67]. Above this concentration, H_2/CO ratio became more than one indicating that either CO is being consumed by the Boudouard reaction, or CO_2 activity is being inhibited yielding to low CO production [66].

Long run experiments (>20 hrs.) for six catalysts with different sulfur concentrations was done to see the effect of sulfur with time. Figure (X) shows the results of methane conversion (a), CO_2 conversion (b), H_2 yield (c), and CO yield (d).

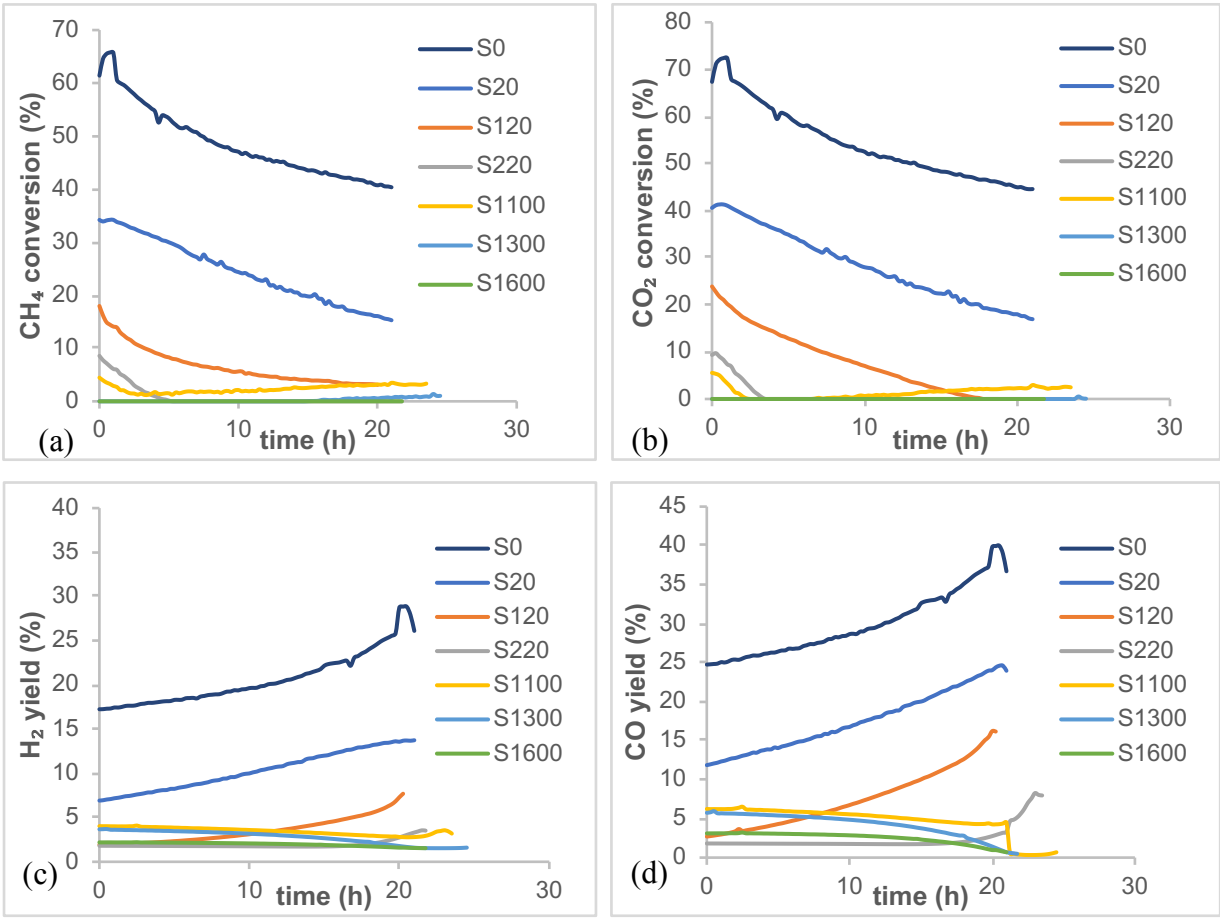

Figure 5- (a) CH_4 conversion, (b) CO_2 conversion, (c) H_2 yield, and (d) CO yield of catalysts with different sulfur concentrations as a function of time.

At low sulfur concentrations of 20 ppm, 120 ppm, and 220 ppm, methane and CO_2 conversions decreased as time passed due to the formation of carbon that blocked the active sites for the reforming reaction [68]. In equivalent, the increase in CO yield as time passes suggests that RGWS reaction is proceeding.

At high sulfur concentrations of (>1100 ppm), the conversions increased with time after 5 hrs. The increase in CO_2 conversion with time associated with slight decrease in CO yield showed that at high sulfur coverages, the Boudouard reaction was dominating and lead to production of CO_2. As time passed, the C produced blocked the

available some active sites leading to inhibition of the Boudouard reaction; thus, CO_2 conversion increased again. As for the very low methane conversion with the significant H_2 yield might be due to production of methane by methanation reaction 5.

$$CO + 3H_2 \rightarrow CH_4 + H_2O \quad (5)$$

It is thus the combination of both reactions the Boudouard, predominantly, and the methanation, to some extent, that resulted in a H_2/CO ratio higher than unity for high sulfur concentrations [66].

D. Characterization of Spent Catalysts

1. TGA Analysis

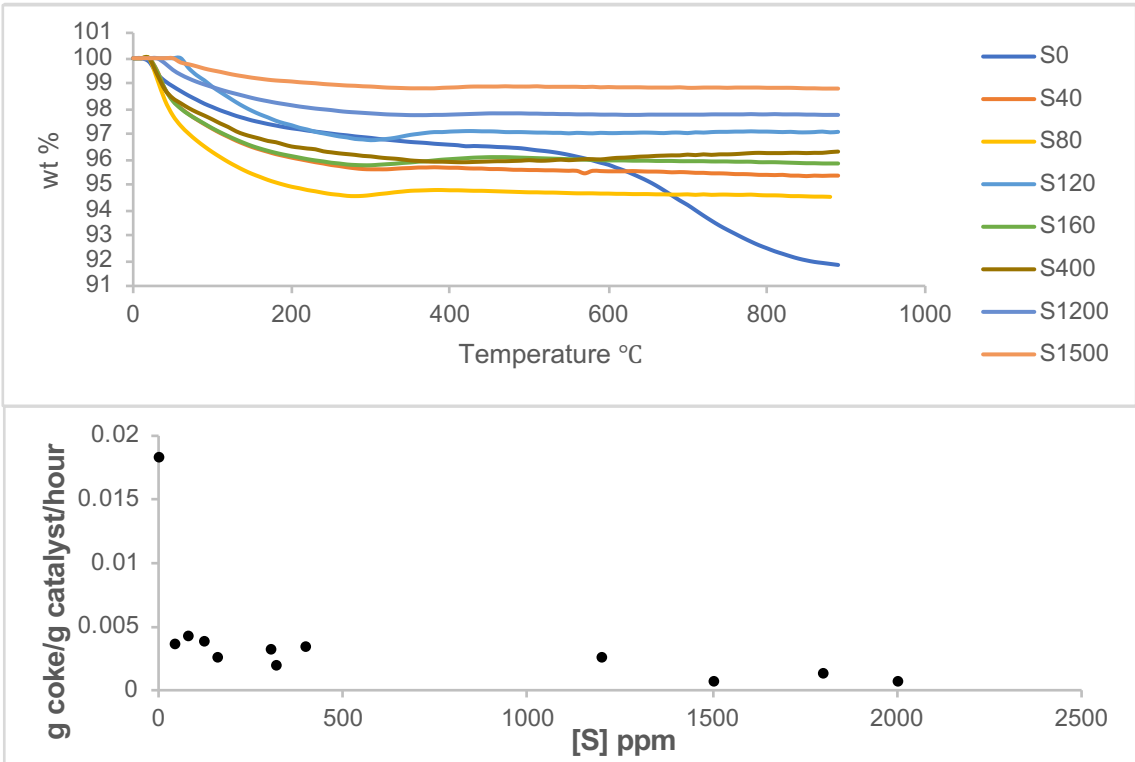

Figure 6- TGA results of spent catalyst with different sulfur concentrations (a) weight loss as function of temperature (b) coke formed as function of sulfur concentration

Figure 6 shows the TGA results of spent catalysts with different sulfur concentration. Graph in figure 6-a represents the loss in catalyst weight percent as function of increasing temperature. For all samples, the initial weight loss up to 300 °C can be assigned to the thermal desorption of water and volatile species, such as CO2 and CO [68]. As for the decrease of weight from 400 to 900 °C it was due to decomposition of the coke on the surface of catalysts [69, 70].

The amount of coke produced on the surface of each catalyst was estimated by equation 10

$$coke\ amount\left(\frac{g}{g_{cat}}\Big/h\right)=\frac{\left(\frac{M1-M2}{100}\right)}{\tau} \tag{10}$$

where M1 represents the weight percent of spent catalyst after desorption of water, M2 represents the weight percent of coked catalyst after burning off the coke [69], and τ is run time of the catalyst in the reformer. The coke amounts produced at different sulfur concentrations are presented in figure 6-b.

For the catalyst with no sulfur content, the amount of coke that was present on the nickel surface was 0.0183g/g_{cat}/h. This amount dropped by 80% to 0.0036g/g_{cat}/h. for only 40 ppm sulfur concentration. At this concentration, the conversion of methane and CO_2 dropped by only by 43% and 46% respectively from conversions corresponding to zero sulfur content. This reflects the fact that the ensemble for the reforming reaction is smaller than that required for nucleation of the carbon [71]. As the sulfur concentration increased, the coke deposited decreased till it became almost zero for 1500 ppm and above. This is due to the decrease in the reforming rate.

2. *SEM results*

Figure 7 represents the SEM images for spent catalyst with different sulfur concentrations. Carbon whiskers are clearly seen in figure 7-a which is the spent catalyst with no sulfur content. For spent catalyst with 80 ppm sulfur (12 % coverage), very few numbers of whiskers are seen indicating that the carbon nucleation was minimized. Those whiskers has less developed structure and they are called "octopus carbon" which are several whiskers growing from one nickel crystal as a result of methane decomposition over passivated sulfur [72]. Rostrup-Nielsen observed octopus carbon as well with sulfur coverages above 66% [10].

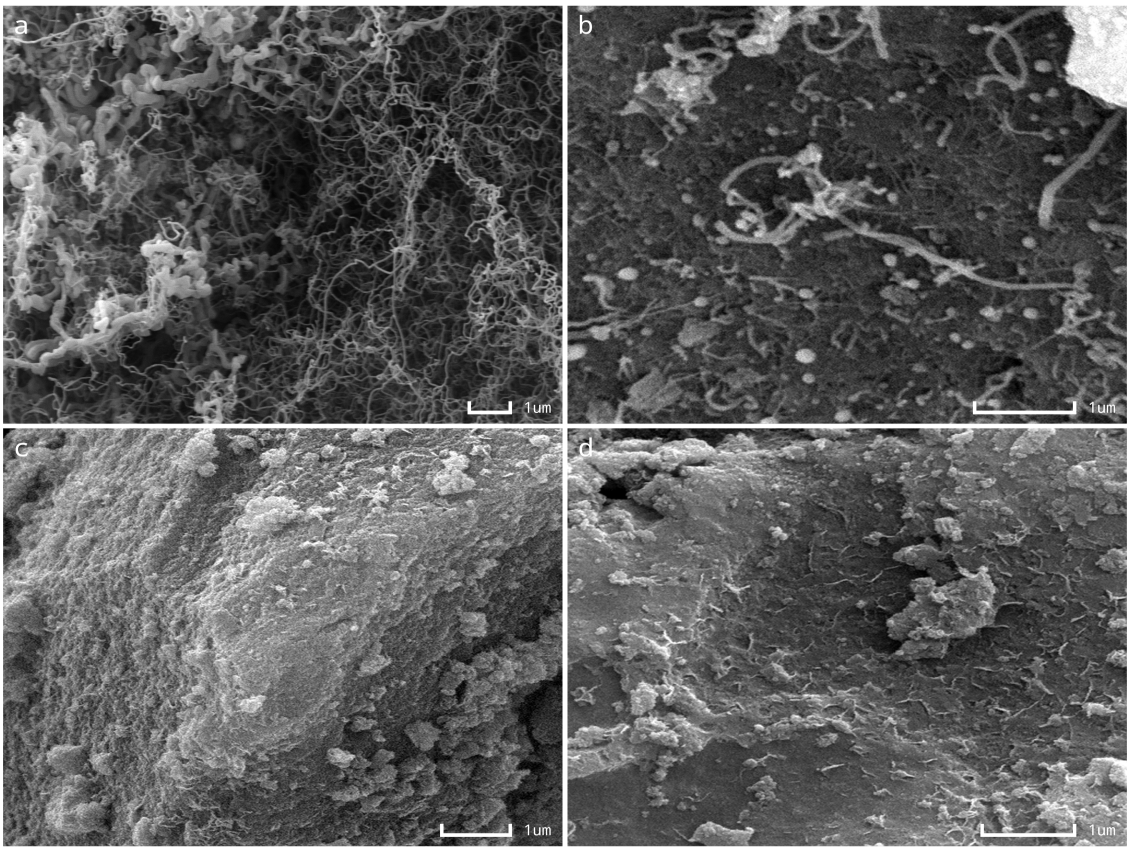

Figure 7- SEM Images of Spent Catalyst (a) S_0, (b) S_{80}, (c) S_{160}, and (d) S_{1500}

No whisker carbon was seen on spent catalysts with higher sulfur contents of 160 ppm and 1500 ppm, represented in figures 7-c and 7-d respectively, indicating that carbon nucleation was inhibited for 23% sulfur coverage and above. This coverage is equivalent to 70% coverage with H_2S [10].

E. Choosing the Best Catalyst

The best sulfur coverage corresponds to the catalyst with high conversion and low coke formation. Figure 8 represents both methane conversion and amount of coke formed on sulfur passivated catalysts at different sulfur concentrations.

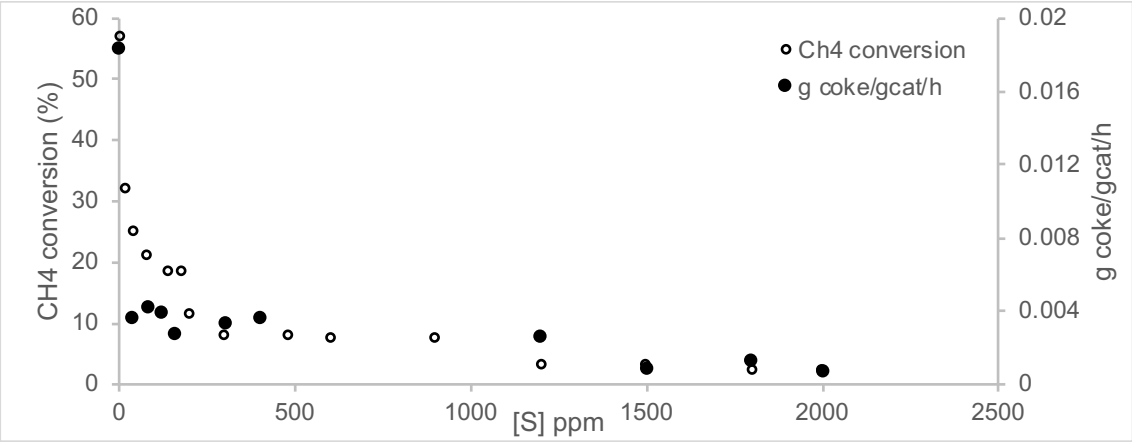

Figure 8- Methane conversion and coke formed as a function of sulfur concentration

For a sulfur concentration of 40 ppm, the conversion decreased by about 43 % while coke formation decreased by 80% compared to the conversion and coke formation when no sulfur was added. As sulfur concentration increased, the conversion decreased rapidly while coke formation decreased slowly. At the sulfur concentration of 1500 ppm and above, both conversion and coke formation lost around 95% of their initial values corresponding to the catalyst with no sulfur added. So, the effect of

increasing sulfur concentration was significant on decreasing the methane conversion but not as effective on coke formation.

Therefore, low sulfur concentrations, less than 80 ppm, are more convenient. SEM pictures for 80 ppm (figure 7-b) showed less developed whiskers that are not harmful for the catalyst. Therefore, the optimum sulfur concentration is 80 ppm which corresponds to 12 % coverage. This value is much less than that found by Rostrup-Nielsen which was 70 % coverage with H_2S [10].

CHAPTER V

CONCLUSION

In this work, a new method to dope a catalyst with sulfur in liquid phase without the use of toxic H_2S was proposed. Liquid phase sulfur adsorption isotherm on nickel catalyst was explained by Langmuir's model. The addition of sulfur on the catalyst affected the morphology by changing the surface area and porosity and caused a drop in the catalyst activity.

RWGS reaction co-existed with the DRM reaction at low sulfur concentrations (<300 ppm). However, at higher sulfur concentrations, two possibilities were proposed: the inhibition of RWGS reaction allowing the Boudouard reaction to take place, or the decrease in CO_2 conversion as a result of change in the morphology of the support. Further research should be done to clarify this.

As for the carbon formation, it was more drastically reduced in the presence of sulfur compared to reduction in activity. The stability on the other hand was not greatly affected by increased sulfur content.

Finally, a sulfur concentration of 80 ppm, corresponding to 12 % coverage, was found to be optimal. Although the at activity was low, there was 80 % drop in carbon formation and the carbon formed was in the form of undeveloped whiskers. Below this coverage, whiskers were still formed, and above this coverage, the activity was severely reduced. The optimal coverage deduced in this work does not correspond to the optimal coverage obtained from gas-phase results in literature.

Further work should be done to understand more the effect of high sulfur concentrations on the kinetics and mechanism of the reaction. Moreover, the liquid phase sulfur passivated catalyst could be tested under SPARG conditions, i.e. by

introducing steam to the DRM process hopping to get higher conversions and better results.

REFERENCES

1. Carriveau, R. and D.S.K. Ting, *1. Hydrogen Storage and Compression*, in *Methane and Hydrogen for Energy Storage*. Institution of Engineering and Technology.
2. Dębek, R., et al., *A Short Review on the Catalytic Activity of Hydrotalcite-Derived Materials for Dry Reforming of Methane.* Catalysts, 2017. **7**(1): p. 32.
3. Abbas, H.F. and W.M.A. Wan Daud, *Hydrogen production by methane decomposition: A review.* International Journal of Hydrogen Energy, 2010. **35**(3): p. 1160-1190.
4. Shekhawat, D., J.J. Spivey, and D.A. Berry, *7. Dry (CO2) Reforming*, in *Fuel Cells - Technologies for Fuel Processing*. Elsevier.
5. Abdullah, B., N.A.A. Ghani, and D.-V.N. Vo, *Recent Advances in Dry Reforming of Methane over Ni-based Catalysts.* Journal of Cleaner Production, 2017.
6. Wurzel, T., S. Malcus, and L. Mleczko, *Reaction engineering investigations of CO 2 reforming in a fluidized-bed reactor.* Chemical Engineering Science, 2000. **55**(18): p. 3955-3966.
7. Rostrup-Nielsen, J.R., J. Sehested, and J.K. Nørskov, *Hydrogen and synthesis gas by steam-and C0 2 reforming.* Advances in catalysis, 2002. **47**: p. 65-139.
8. Joshi, S.S. and V.V. Ranade, *5.3.1.2 Coke Formation during Dry (CO2) Reforming Reaction*, in *Industrial Catalytic Processes for Fine and Specialty Chemicals*. Elsevier.
9. Ginsburg, J.M., et al., *Coke formation over a nickel catalyst under methane dry reforming conditions: thermodynamic and kinetic models.* Industrial & engineering chemistry research, 2005. **44**(14): p. 4846-4854.
10. Rostrup-Nielsen, J.R., *Sulfur-passivated nickel catalysts for carbon-free steam reforming of methane.* Journal of Catalysis, 1984. **85**(1): p. 31-43.
11. Erley, W. and H. Wagner, *Sulfur poisoning of carbon monoxide adsorption on Ni (111).* Journal of Catalysis, 1978. **53**(3): p. 287-294.
12. Tsakoumis, N.E., et al., *Deactivation of cobalt based Fischer–Tropsch catalysts: A review.* Catalysis Today, 2010. **154**(3): p. 162-182.
13. Kim, J.-H., et al., *Effect of metal particle size on coking during CO 2 reforming of CH 4 over Ni–alumina aerogel catalysts.* Applied Catalysis A: General, 2000. **197**(2): p. 191-200.
14. Min, J.-E., et al., *Carbon dioxide reforming of methane on Ni–MgO–Al2O3 catalysts prepared by sol–gel method: Effects of Mg/Al ratios.* Journal of Industrial and Engineering Chemistry, 2015. **26**: p. 375-383.
15. Hu, Y.H., *Advances in catalysts for CO2 reforming of methane*, in *Advances in CO2 Conversion and Utilization*. 2010, ACS Publications. p. 155-174.
16. Niu, J., et al., *Dry (CO 2) reforming of methane over Pt catalysts studied by DFT and kinetic modeling.* Applied Surface Science, 2016. **376**: p. 79-90.
17. Tomishige, K., Y.-g. Chen, and K. Fujimoto, *Studies on Carbon Deposition in CO2Reforming of CH4over Nickel–Magnesia Solid Solution Catalysts.* Journal of Catalysis, 1999. **181**(1): p. 91-103.
18. Horiuchi, T., et al., *Suppression of carbon deposition in the CO2-reforming of CH4 by adding basic metal oxides to a Ni/Al2O3 catalyst.* Applied Catalysis A: General, 1996. **144**(1-2): p. 111-120.

19. Roh, H.-S. and K.-W. Jun, *Carbon dioxide reforming of methane over Ni catalysts supported on Al2O3 modified with La2O3, MgO, and CaO.* Catalysis surveys from Asia, 2008. **12**(4): p. 239-252.
20. Sehested, J., *Four challenges for nickel steam-reforming catalysts.* Catalysis Today, 2006. **111**(1–2): p. 103-110.
21. Nikoo, M.K. and N.A.S. Amin, *Thermodynamic analysis of carbon dioxide reforming of methane in view of solid carbon formation.* Fuel Processing Technology, 2011. **92**(3): p. 678-691.
22. Goodman, D.W. and M. Kiskinova, *Chemisorption and reactivity studies of H2 and CO on sulfided Ni(100).* Surface Science Letters, 1981. **105**(2): p. L265-L270.
23. Rostrup-Nielsen, J.R. and K. Pedersen, *Sulfur poisoning of Boudouard and methanation reactions on nickel catalysts.* Journal of Catalysis, 1979. **59**(3): p. 395-404.
24. Trimm, D.L., *Catalysts for the control of coking during steam reforming.* Catalysis Today, 1999. **49**(1–3): p. 3-10.
25. Mortensen, P. and I. Dybkjær, *Industrial scale experience on steam reforming of CO2-rich gas*. Vol. 495. 2015.
26. Aramouni, N.A.K., et al., *Thermodynamic analysis of methane dry reforming: Effect of the catalyst particle size on carbon formation.* Energy Conversion and Management, 2017. **150**: p. 614-622.
27. Bartholomew, C.H., P.K. Agrawal, and J.R. Katzer, *Sulfur Poisoning of Metals.* Advances in Catalysis, 1982. **31**: p. 135-242.
28. Bartholomew, C.H., *Mechanisms of catalyst deactivation.* Applied Catalysis A: General, 2001. **212**(1): p. 17-60.
29. Sehested, J., et al., *Sintering of nickel steam-reforming catalysts: effects of temperature and steam and hydrogen pressures.* Journal of Catalysis, 2004. **223**(2): p. 432-443.
30. Azzam, M., et al., *Dynamic optimization of dry reformer under catalyst sintering using neural networks.* Energy Conversion and Management, 2018. **157**: p. 146-156.
31. Jafarbegloo, M., et al., *One-pot synthesis of NiO–MgO nanocatalysts for CO 2 reforming of methane: The influence of active metal content on catalytic performance.* Journal of Natural Gas Science and Engineering, 2015. **27**: p. 1165-1173.
32. Aasberg-Petersen, K., et al., *Synthesis gas production for FT synthesis.* Studies in Surface Science and Catalysis, 2004. **152**: p. 258-405.
33. Perdereau, M. and J. Oudar, *Structure, mécanisme de formation et stabilité de la couche d'adsorption du soufre sur le nickel.* Surface Science, 1970. **20**(1): p. 80-98.
34. Bartholomew, C., G. Weatherbee, and G. Jarvi, *Sulfur poisoning of nickel methanation catalysts: I. in situ deactivation by H2S of nickel and nickel bimetallics.* Journal of Catalysis, 1979. **60**(2): p. 257-269.
35. Martin, G., M. Primet, and J. Dalmon, *Reactions of CO and CO2 on NiSiO2 above 373 K as studied by infrared spectroscopic and magnetic methods.* Journal of Catalysis, 1978. **53**(3): p. 321-330.
36. Araki, M. and V. Ponec, *Methanation of carbon monoxide on nickel and nickel-copper alloys.* Journal of Catalysis, 1976. **44**(3): p. 439-448.

37. Yu, K., D. Ling, and W. Spicer, *Thermal desorption studies of CO and H2 from the Cu Ni alloy.* Journal of Catalysis, 1976. **44**(3): p. 373-384.
38. Bond, G.C. and B.D. Turnham, *The kinetics and mechanism of carbon monoxide hydrogenation over silica-supported ruthenium-copper catalysts.* Journal of Catalysis, 1976. **45**(2): p. 128-136.
39. Alstrup, I. and N.T. Andersen, *Statistical models for ensemble control by alloying and poisoning of catalysts: II. Comparisons with Monte Carlo simulations and with experimental results.* Journal of Catalysis, 1987. **104**(2): p. 466-479.
40. Stal, J., et al., *Sulfur-Passivated Reforming Process Lowers Syngas Hydrogen.* Carbon Ratio. Oil Gas J, 1992. **90**: p. 62.
41. Roussière, T.L., *Catalytic Reforming of Methane in the Presence of CO2 and H2O at High Pressure*. 2013, KIT-Bibliothek.
42. Udengaard, N.R., *Sulfur passivated reforming process lowers syngas H sub 2/CO ratio.* Oil and Gas Journal;(United States), 1992. **90**(10).
43. Mortensen, P.M. and I. Dybkjær, *Industrial scale experience on steam reforming of CO2-rich gas.* Applied Catalysis A: General, 2015. **495**: p. 141-151.
44. Rezgui, S. and B.C. Gates, *Control of magnesia–alumina properties by acetic acid in sol–gel synthesis.* Journal of non-crystalline solids, 1997. **210**(2): p. 287-297.
45. Othman, M., N. Rasid, and W. Fernando, *Effects of thermal treatment on the micro-structures of co-precipitated and sol–gel synthesized (Mg–Al) hydrotalcites.* Microporous and mesoporous materials, 2006. **93**(1): p. 23-28.
46. Uvarov, V. and I. Popov, *Metrological characterization of X-ray diffraction methods for determination of crystallite size in nano-scale materials.* Materials characterization, 2007. **58**(10): p. 883-891.
47. Mishra, A.K., *3.2.1 Chemical Precipitation*, in *Nanomaterials for Water Remediation - Carbon-Based Materials, Volume 1*. Smithers Rapra Technology.
48. Ma, L. and R.T. Yang, *Selective adsorption of sulfur compounds: Isotherms, heats, and relationship between adsorption from vapor and liquid solution.* Industrial & engineering chemistry research, 2007. **46**(9): p. 2760-2768.
49. Frank, R.B., et al., *INORGANIC NONMETALLIC SUBSTANCES*, in *Environmental Monitoring Handbook*. 2002, McGraw Hill Professional, Access Engineering.
50. Kirkpatrick, W.J., *Nickel Sulfide Catalysts**Contribution from The International Nickel Company Fellowship, Mellon Institute, Pittsburgh, Pa.* Advances in Catalysis, 1951. **3**: p. 329-339.
51. Den Besten, I. and P. Selwood, *The chemisorption of hydrogen sulfide, methyl sulfide, and cyclohexene on supported nickel catalysts.* Journal of catalysis, 1962. **1**(2): p. 93-102.
52. Rostrup-Nielsen, J.R., *Chemisorption of hydrogen sulfide on a supported nickel catalyst.* Journal of Catalysis, 1968. **11**(3): p. 220-227.
53. Bolis, V., *Fundamentals in adsorption at the solid-gas interface. Concepts and thermodynamics*, in *Calorimetry and Thermal Methods in Catalysis*. 2013, Springer. p. 3-50.
54. Do, D.D., *Adsorption analysis: equilibria and kinetics*. Vol. 2. 1998: Imperial college press London.

55. Oliphant, J.L., et al., *Chemisorption of hydrogen sulfide on nickel and ruthenium catalysts.* Journal of Catalysis, 1978. **51**(2): p. 229-242.
56. Alstrup, I., J.R. Rostrup-Nielsen, and S. Røen, *High temperature hydrogen sulfide chemisorption on nickel catalysts.* Applied Catalysis, 1981. **1**(5): p. 303-314.
57. Wang, J.-H. and M. Liu, *Computational study of sulfur–nickel interactions: A new S–Ni phase diagram.* Electrochemistry Communications, 2007. **9**(9): p. 2212-2217.
58. Amin, M.H., et al., *Highly stable ytterbium promoted Ni/γ-Al2O3 catalysts for carbon dioxide reforming of methane.* Applied Catalysis B: Environmental, 2012. **119–120**: p. 217-226.
59. Aghamohammadi, S., et al., *Sequential impregnation vs. sol-gel synthesized Ni/Al2O3-CeO2 nanocatalyst for dry reforming of methane: Effect of synthesis method and support promotion.* Molecular Catalysis, 2017. **431**: p. 39-48.
60. Monshi, A., M.R. Foroughi, and M.R. Monshi, *Modified Scherrer equation to estimate more accurately nano-crystallite size using XRD.* World Journal of Nano Science and Engineering, 2012. **2**(3): p. 154-160.
61. Yu, T.-C. and H. Shaw, *The effect of sulfur poisoning on methane oxidation over palladium supported on γ-alumina catalysts.* Applied Catalysis B: Environmental, 1998. **18**(1): p. 105-114.
62. Lv, X., et al., *A highly dispersed nickel supported catalyst for dry reforming of methane.* Catalysis Communications, 2012. **20**: p. 6-11.
63. Barroso Quiroga, M.M. and A.E. Castro Luna, *Kinetic analysis of rate data for dry reforming of methane.* Industrial & engineering chemistry research, 2007. **46**(16): p. 5265-5270.
64. González, A.R., et al., *Dry reforming of methane on Ni–Mg–Al nano-spheroid oxide catalysts prepared by the sol–gel method from hydrotalcite-like precursors.* Applied Surface Science, 2013. **280**: p. 876-887.
65. Rostrup-Nielsen, J. and D.L. Trimm, *Mechanisms of carbon formation on nickel-containing catalysts.* Journal of Catalysis, 1977. **48**(1): p. 155-165.
66. Sivaiah, M.V., et al., *Nickel based catalysts derived from hydrothermally synthesized 1:1 and 2:1 phyllosilicates as precursors for carbon dioxide reforming of methane.* Microporous and Mesoporous Materials, 2011. **140**(1): p. 69-80.
67. Therdthianwong, S., et al., *Synthesis gas production from dry reforming of methane over Ni/Al2O3 stabilized by ZrO2.* International Journal of Hydrogen Energy, 2008. **33**(3): p. 991-999.
68. Al-Swai, B.M., N.B. Osman, and B. Abdullah, *Catalytic performance of Ni/MgO catalyst in methane dry reforming.* AIP Conference Proceedings, 2017. **1891**(1).
69. Song, Y., et al., *Partial Oxidation of Methane to Syngas over Ni/Al2O3 Catalysts Prepared by a Modified Sol− Gel Method.* Energy & Fuels, 2009. **23**(4): p. 1925-1930.
70. Tsyganok, A.I., et al., *Dry reforming of methane over catalysts derived from nickel-containing Mg–Al layered double hydroxides.* Journal of Catalysis, 2003. **213**(2): p. 191-203.
71. Rostrup-Nielsen, J., *Aspects of CO 2-reforming of methane.* Studies in surface science and catalysis, 1994. **81**: p. 25-41.

72. Rostrup-Nielsen, J.R. and J. Sehested, *Whisker Carbon Revisited*, in *Studies in Surface Science and Catalysis*, G.W.R. J.J. Spivey and B.H. Davis, Editors. 2001, Elsevier. p. 1-12.